Controlling the signal angular profile in a Bessel-beam-pumped optical parametric amplifier

V. Pyragaite,* V. Smilgevičius, R. Butkus, A. Narmontas, A. Stabinis, and A. Piskarskas
Department of Quantum Electronics, Vilnius University, Saulėtekio Avenue 9, Building 3, LT-10222 Vilnius, Lithuania
(Received 4 April 2014; published 7 August 2014)

An optical parametric amplifier pumped by a Bessel beam is investigated. It is revealed that under propagation in a nonlinear crystal, the signal angular profile after a transient process does not depend on the input profile and the signal beam becomes localized in the pump field. The control of the output signal angular profile by variation of the pump cone angle and intensity is demonstrated. The effect is elucidated by the numerical simulations as well as experiment. The explanation by the derived eigenvalue problem is given.

DOI: 10.1103/PhysRevA.90.023807 PACS number(s): 42.65.Yj

I. INTRODUCTION

The Bessel beams (BBs) were introduced by Durnin in 1987 [1]. A main feature of BBs is their immunity to diffraction. The wave vectors of BBs lie on a cone surface and its angular spectrum is a ring. Many interesting experiments such as self-healing of a BB and micromanipulation using optical tweezers have been discussed; see Ref. [2] and references therein. The research on nonlinear optics of BBs began with the study of second harmonic generation by a BB in 1993 [3]. Since then, special attention has been paid to the optical parametric processes with a BB pump [4–7]. The optical parametric amplifier (OPA) [4], generator (OPG) [7], and oscillator (OPO) [5,6] were studied. Interestingly, even a distorted BB or, more precisely, incoherent conical beam can parametrically amplify a coherent signal beam [4]. The incoherence of the conical pump can be transferred to the generated idler conical beam [5]. Such experiments confirm the idea of the parametric combining [8]. In Ref. [8], the parametric amplification of a single signal beam by several intersecting pump beams was demonstrated. The incoherent BB can be described as a superposition of a large number of intersecting incoherent beams [9].

The parametric amplification by a BB is specific since, in this case, the pump intensity is not smooth because the BB obeys a sharp peak at the center and vanishing oscillations around it. In this case, the transverse phase matching of interacting beams conditions the output angular spectrum of the axial signal and conical idler beams [4]; see Fig. 1. It seems that only the signal beam propagating along the pump cone axis can be simultaneously phase matched with all plane waves that constitute the conical pump beam. For this reason, an acceptance angle of OPA pumped by a BB should decrease under propagation in a nonlinear crystal. Here, we study the parametric amplification of an injected signal beam in the field of the BB pump in order to determine the acceptance angle of the OPA and to elucidate how it can be controlled by the parameters of the pump beam: BB cone angle and intensity.

The paper is organized as follows. In Sec. II, the governing equations and the results of their simulation are presented. The nonlinear coupling equations and the derived eigenvalue problem as well as its solution by the iterative method are introduced. In Sec. III, the experiment of the amplification of the signal beam by the Bessel beam in the OPA is described. Finally, in Sec. IV, the conclusions are drawn.

II. THEORETICAL DETAILS

A. Nonlinear coupling equations

In the case of noncritical phase matching, the nonlinear coupling equations for signal (1), idler (2), and pump (3) beams propagating in the z direction read

$$\begin{aligned}
&\frac{\partial A_1}{\partial z}+\frac{i}{2k_1}\left(\frac{\partial^2 A_1}{\partial x^2}+\frac{\partial^2 A_1}{\partial y^2}\right)=\sigma_1 A_2^* A_3\exp(-i\Delta z),\\
&\frac{\partial A_2}{\partial z}+\frac{i}{2k_2}\left(\frac{\partial^2 A_2}{\partial x^2}+\frac{\partial^2 A_2}{\partial y^2}\right)=\sigma_2 A_1^* A_3\exp(-i\Delta z),\\
&\frac{\partial A_3}{\partial z}+\frac{i}{2k_3}\left(\frac{\partial^2 A_3}{\partial x^2}+\frac{\partial^2 A_3}{\partial y^2}\right)=-\sigma_3 A_1 A_2\exp(i\Delta z),
\end{aligned}\tag{1}$$

where A, k, and Δ are the complex amplitude, wave number, and phase mismatch, respectively. (x,y,z) are the Cartesian coordinates. σ is a nonlinear coupling coefficient. We assume that all optical fields are axially symmetric and that there is no pump depletion and diffraction. Then, in the case of a Bessel-Gauss (BG) pump beam,

$$A_3=a_{30}\exp\left(-r^2/d_3^2\right)J_0(\beta_0 r)\exp\left(i\beta_0^2 z/2k_3\right),\tag{2}$$

where $J_0(\beta_0 r)$ is a zero-order Bessel function, $\beta_0=k_3\alpha_3$, and $2\alpha_3$ is a pump cone angle (Fig. 1). $r=\sqrt{x^2+y^2}$ and a_{30} is a pump amplitude. At the input of the crystal, $z=0$, the amplitudes of signal and idler read

$$\begin{aligned}
&A_1(z=0,r)=a_{10}\exp\left(-r^2/d_0^2\right),\\
&A_2(z=0,r)=0,
\end{aligned}\tag{3}$$

where a_{10} is a signal amplitude and d_0 is a beam radius. Further we assume an exact noncollinear phase matching of Gaussian signal beam with the conical pump and idler beams. In this case, due to nonlinear Snell's law [10], the components of the wave vectors $\mathbf{k}_2$ and $\mathbf{k}_3$ in the xy plane are the same (β_0) and, as a result, for the phase mismatch Δ, we obtain $\Delta=\frac{\beta_0^2}{2}(\frac{1}{k_3}-\frac{1}{k_2})$. Further, we make use of Hankel transform:

$$\begin{aligned}
&S(\beta)=2\pi\int_0^\infty r A(r)J_0(\beta r)dr,\\
&A(r)=\frac{1}{2\pi}\int_0^\infty \beta S(\beta)J_0(\beta r)d\beta.
\end{aligned}\tag{4}$$

*viktorija.pyragaite@ff.vu.lt

 ©2014 American Physical Society

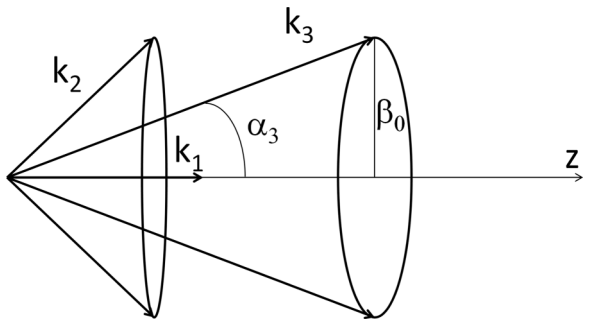

FIG. 1. Schematic depiction of conical pump (wave number k_3), axial signal (k_1), and conical idler (k_2) beams.

Here, $S(\beta)$ is a spectral amplitude. Function $|S(\beta)|^2$ is an angular spectrum. From Eqs. (1), one obtains

$$\begin{aligned}\frac{\partial S_1}{\partial z}-\frac{i}{2k_1}\beta_1^2 S_1 &= \frac{2\pi}{L_n}\sqrt{\frac{\sigma_1}{\sigma_2}}\exp\left(i\beta_0^2 z/2k_2\right)\int_0^\infty rA_2^*(r)\\ &\quad\times J_0(\beta_0 r)J_0(\beta_1 r)\exp\left(-r^2/d_3^2\right)dr,\\ \frac{\partial S_2}{\partial z}-\frac{i}{2k_2}\beta_2^2 S_2 &= \frac{2\pi}{L_n}\sqrt{\frac{\sigma_2}{\sigma_1}}\exp\left(i\beta_0^2 z/2k_2\right)\int_0^\infty rA_1^*(r)\\ &\quad\times J_0(\beta_0 r)J_0(\beta_2 r)\exp\left(-r^2/d_3^2\right)dr. \quad (5)\end{aligned}$$

Here, $L_n=1/(\sqrt{\sigma_1\sigma_2}a_{30})$ is a characteristic length of nonlinear interaction. After insertion of $A_1^*(r)$ and $A_2^*(r)$, one obtains

$$\begin{aligned}l\frac{\partial S_1}{\partial z}-\frac{i}{2k_1}\beta_1^2 S_1 &= \frac{1}{L_n}\sqrt{\frac{\sigma_1}{\sigma_2}}\exp\left(i\beta_0^2 z/2k_2\right)\\ &\quad\times\int_0^\infty \beta_2 S_2^*(\beta_2)F(\beta_1,\beta_2)d\beta_2,\\ \frac{\partial S_2}{\partial z}-\frac{i}{2k_2}\beta_2^2 S_2 &= \frac{1}{L_n}\sqrt{\frac{\sigma_2}{\sigma_1}}\exp\left(i\beta_0^2 z/2k_2\right)\\ &\quad\times\int_0^\infty \beta_1 S_1^*(\beta_1)F(\beta_1,\beta_2)d\beta_1, \quad (6)\end{aligned}$$

where F is a transverse phase-matching integral,

$$F(\beta_1,\beta_2)=\int_0^\infty r\exp\left(-r^2/d_3^2\right)J_0(\beta_1 r)J_0(\beta_2 r)J_0(\beta_0 r)dr. \quad (7)$$

Boundary conditions at $z=0$ are the following:

$$\begin{aligned}S_1(z=0,\beta_1)&=S_{10}(\beta_1)=\pi a_{10}d_0^2\exp\left(-\beta_1^2 d_0^2/4\right),\\ S_2(z=0,\beta_2)&=S_{20}(\beta_2)=0.\end{aligned} \quad (8)$$

Let us seek for the solutions of Eqs. (6) in the form

$$\begin{aligned}S_1(z,\beta_1)&=f_1(\beta_1)\exp(\Gamma z),\\ S_2(z,\beta_2)&=f_2(\beta_2)\exp\left(\Gamma^* z+i\beta_0^2 z/2k_2\right),\end{aligned} \quad (9)$$

where $f_{1,2}=|f_{1,2}|\exp(i\Psi_{1,2})$. The functions $|f_{1,2}|$ are the angular profiles, $\Psi_{1,2}$ are the spectral phases of signal and idler beams, and $\mathrm{Re}(\Gamma)$ is an increment, i.e., the spectral amplitudes $S_{1,2}$ of signal and idler beams grow exponentially with z as $\exp[\mathrm{Re}(\Gamma)z]$. $\mathrm{Re}(\cdot)$ denotes a real part. We arrive at the eigenvalue problem:

$$\begin{aligned}&\left(\Gamma-i\frac{\beta_1^2}{2k_1}\right)f_1(\beta_1)\\ &\quad=\frac{1}{L_n}\sqrt{\frac{\sigma_1}{\sigma_2}}\int_0^\infty \beta_2 f_2^*(\beta_2)F(\beta_1,\beta_2)d\beta_2,\\ &\left(\Gamma^*-i\frac{\beta_2^2-\beta_0^2}{2k_2}\right)f_2(\beta_2)\\ &\quad=\frac{1}{L_n}\sqrt{\frac{\sigma_2}{\sigma_1}}\int_0^\infty \beta_1 f_1^*(\beta_1)F(\beta_1,\beta_2)d\beta_1.\end{aligned} \quad (10)$$

This system of equations can be solved by the method of iterations. One guesses arbitrary $f_{10}(\beta_1)$ and Γ_0 and inserts them into the following equations:

$$\begin{aligned}f_2(\beta_2)&=\frac{1}{\Gamma_0^*-i\frac{\beta_2^2-\beta_0^2}{2k_2}}\frac{1}{L_n}\sqrt{\frac{\sigma_2}{\sigma_1}}\int_0^\infty \beta_1 f_{10}^*(\beta_1)F(\beta_1,\beta_2)d\beta_1,\\ f_1(\beta_1)&=\frac{1}{\Gamma_0-i\frac{\beta_1^2}{2k_1}}\frac{1}{L_n}\sqrt{\frac{\sigma_1}{\sigma_2}}\int_0^\infty \beta_2 f_2^*(\beta_2)F(\beta_1,\beta_2)d\beta_2,\\ \Gamma&=\frac{1}{f_2^*(\beta_0)L_n}\sqrt{\frac{\sigma_2}{\sigma_1}}\int_0^\infty \beta_1 f_1(\beta_1)F(\beta_1,\beta_0)d\beta_1. \quad (11)\end{aligned}$$

After this step, one assumes $\Gamma_0=\Gamma$, $f_{10}=f_1$, and inserts the new values into Eqs. (11) again. We note that the solution of the eigenvalue problem takes much less time than computing the differential equations (6).

B. Numerical simulations

We have simulated Eqs. (6) and the obtained signal and idler beam angular profiles were compared to the profiles $f_{1,2}$, which were obtained from iterative solution of the eigenvalue problem, given by Eqs. (10). The results are presented in Fig. 2. Superscripts "in" and "out" denote the values at the input and output, respectively. Here and in the other figures, all angles are outside the crystal, $\alpha=\beta/k_{10}$, and $\Delta\alpha_1$ is a signal angular spectrum width at FWHM, i.e., $\Delta\alpha_1$ was calculated by taking the width of angular spectrum $|S_1|^2$ at its half maximum. The calculations were performed for a $KTiOPO_4$ (KTP) type-II crystal at pump and signal wavelengths 532 and 1064 nm, respectively. The refractive indices from Ref. [11] were used and noncritical phase matching was assumed due to small walk-off angles in this case.

Note that an output profile of the signal angular spectrum does not depend on the input profile. So, the localization (capture) of signal beam in the OPA pumped by the Bessel beam occurs. This is true even when the input profile is incoherent. In Fig. 2(c), the noisy seed was simulated by means of the method described in [12] for simulation of Gaussian-Gaussian noise. After [12], the noisy amplitude is calculated from

$$A_{10}(x)=a_{10}\frac{1}{\sqrt{N_s}}\exp\left(-\frac{x^2}{d_3^2}\right)\sum_{s=1}^{N_s}\exp(iK_s x-i\xi_s), \quad (12)$$

where K_s are the random numbers of normal distribution with variance $\sqrt{2}/\rho$, where ρ is a correlation radius, and ξ_s is a uniformly distributed phase. The correlation radius $\rho=40$ μm.

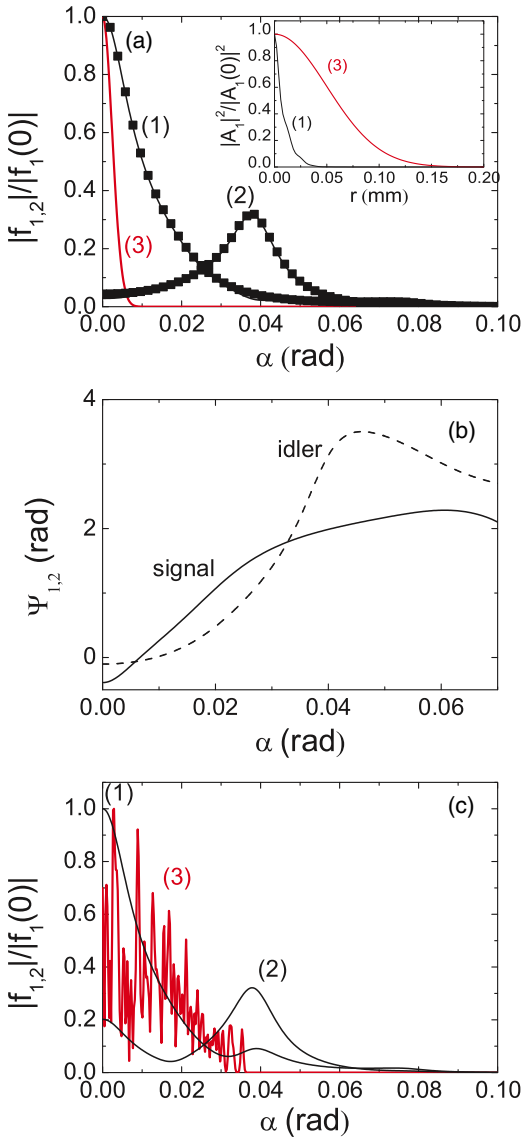

FIG. 2. (Color online) (a),(c) Angular profiles of amplified signal (1) and idler (2) beams. Solution of Eqs. (6) (lines) and Eqs. (10) (squares). (3) (red lines) shows the input signal angular profile. (b) Spectral phase of the signal and idler beams, given by Eqs. (10). (a),(b) Regular and (c) incoherent input. $\Delta\alpha_1^{\text{in}} = 4$ mrad. $\alpha_3 = 0.02$ rad, $d_3 = 800$ μm, $L_n = 350$ μm. z: (a),(b) 1 cm, (c) 2 cm. Squares in (a) and lines in (b): 20 iterations, input $f_{10} = S_{10}$, $\Gamma_0 = 1/L_n$. Inset in (a): input (3) and output (1) signal fields.

The amplitude is truncated by a Gaussian envelope of radius d_3, so Eq. (12) describes a Gaussian Schell-model beam [13]. Input spectrum $S_{10}(\beta_x)$ was calculated by taking the one-dimensional Fourier transform of $A_{10}(x)$. $S_{10}(\beta)$ was obtained by leaving the values at $\beta_x \geqslant 0$.

In Fig. 2(c), the output signal profile is smooth. The idler spectrum part appears in the spectrum of the signal, and vice versa. This does not take place when the input spectrum is rather narrow [Fig. 2(a)]. In Fig. 2(c), the crystal length was taken larger than in Figs. 2(a) and 2(b) because the parametric gain is less in the case of incoherent seed. The phases of the signal and idler beams are depicted in Fig. 2(b).

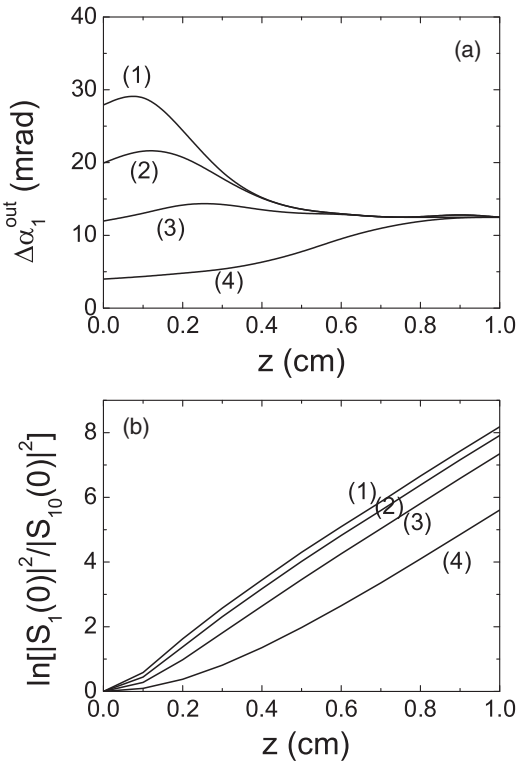

FIG. 3. Dependence of (a) angular spectrum width and (b) parametric gain (at $\beta = 0$) of amplified signal on crystal length. $\alpha_3 = 0.02$ rad, $d_3 = 800$ μm, $L_n = 350$ μm. $\Delta\alpha_1^{\text{in}}$: (1) 28, (2) 20, (3) 12, and (4) 4 mrad. Solutions of Eqs. (6).

The localization of the signal beam can also be seen from Fig. 3. Here the spectrum width $\Delta\alpha_1^{\text{out}}$ and the increment $\text{Re}(\Gamma)$ are depicted. The spectrum width $\Delta\alpha_1^{\text{out}}$ of the amplified signal does not depend on the input spectrum width $\Delta\alpha_1^{\text{in}}$, and the increment becomes the same after a transient process. By transient process, we mean the variation of spectrum width at $z < 0.8$ cm. The value of the spectrum width at the output depends on the pump beam intensity (nonlinear interaction length L_n) and cone angle $2\alpha_3$. The dependence on the nonlinear interaction length is elucidated by Figs. 4 and 5. As we can see, the spectrum width approaches less value when L_n increases, meanwhile the increment becomes smaller. Note that the dependences on z were calculated from Eqs. (6) and the localized values of Fig. 5 were estimated from the eigenvalue problem.

However, the variation of spectrum width before the localization cannot be obtained from the eigenvalue problem (10). Only steady solutions can be extracted from it. We note that a localization of the signal beam in the process of linear parametric amplification was discussed earlier in Refs. [14,15]. The localization is possible when signal and idler beams are propagating in different directions with respect to the pump beam. Under such condition, the outgoing signal and idler beams can be captured by the pump beam and an exponential amplification takes place. A simultaneous temporal and spatial localization of signal and idler pulsed beams occurs under parametric amplification in a degenerate OPA when group-velocity dispersion and diffraction of the pulsed pump beam can be neglected [16]. An angular dispersion inside the

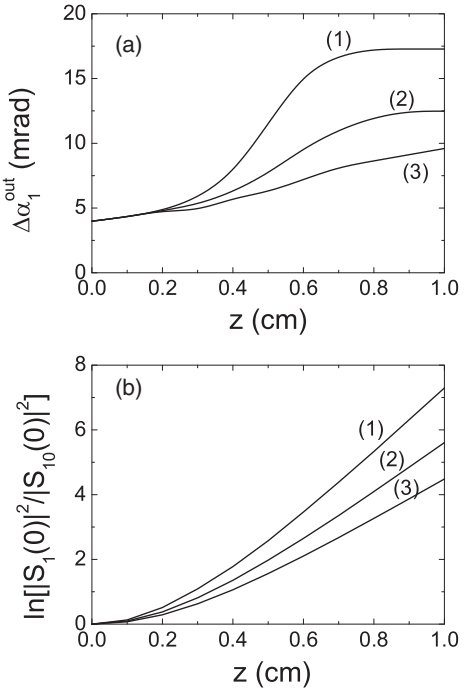

FIG. 4. Dependence of (a) angular spectrum width and (b) parametric gain (at $\beta = 0$) of amplified signal on crystal length. $\alpha_3 = 0.02$ rad, $d_3 = 800$ μm, $\Delta\alpha_1^{in} = 4$ mrad. L_n: (1) 300, (2) 350, (3) 400 μm. Solutions of Eqs. (6).

nonlinear crystal of the OPG coincides with an angular dispersion of localized pulsed beams, which are free of diffraction and dispersion spreading [17], and the parametric amplification of dispersionless and diffractionless polychromatic Bessel beams is possible [18–20].

From Fig. 6, it is evident that the output signal spectrum width decreases when the cone angle of the pump beam increases [compare curves (1) and (2)]. Within the given range of the input spectrum width, the spectrum width of the amplified signal does not change. This range involves the values which are much smaller and much larger than the value for the amplified signal. The spectrum width does not change when the beam radius of the pump beam varies; see Fig. 7.

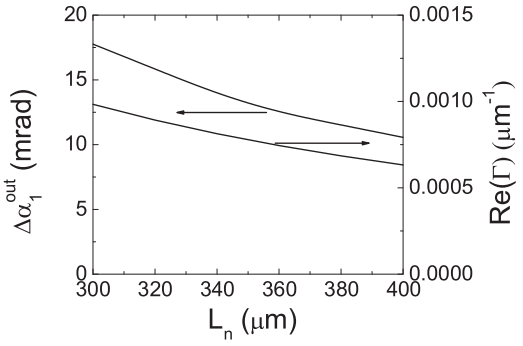

FIG. 5. Dependence of signal angular spectrum width and increment on the nonlinear interaction length. $\alpha_3 = 0.02$ rad, $d_3 = 800$ μm, $\Delta\alpha_1^{in} = 4$ mrad. Solutions of Eqs. (10), 20 iterations, input $f_{10} = S_{10}$, $\Gamma_0 = 1/L_n$.

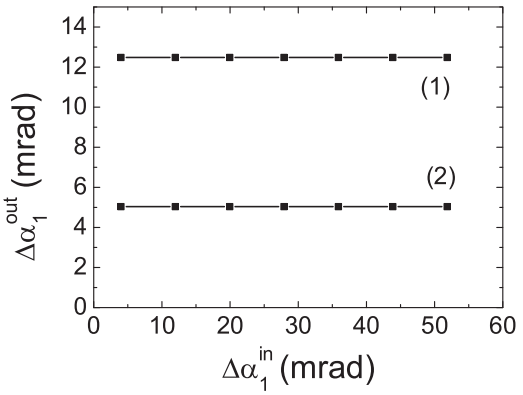

FIG. 6. Dependence of signal angular spectrum width on input signal spectrum width. (1) $\alpha_3 = 0.02$ rad and (2) 0.03 rad. $d_3 = 800$ μm, $L_n = 350$ μm, $z = 1$ cm. Solutions of Eqs. (6).

Of course, at very small radius d_3 of the BG pump beam, this result does not hold because considerable diffraction of the pump beam would take place in this case.

We note that the obtained results are valid when the diffraction of the BG beam can be neglected. Further we shall determine a characteristic diffraction length L_B of the BG beam. The diffraction properties of BG beams were discussed earlier in Ref. [21]. In the case of free propagation of the BG pump beam, its angular spectrum is described by equation

$$S_3(\beta,z) = S_{30}(\beta)\exp(i\beta^2 z/2k_3), \tag{13}$$

where

$$S_{30}(\beta) = S_3(\beta,0) = 2\pi a_0 \int_0^\infty r\exp\left(-r^2/d_3^2\right) J_0(\beta_0 r) J_0(\beta r) dr. \tag{14}$$

An axial amplitude of diffracting BG beam reads

$$A_3(0,z) = \frac{1}{2\pi}\int_0^\infty \beta S_3(\beta,z) d\beta. \tag{15}$$

An integration in Eqs. (14) and (15) yields

$$A_3(0,z) = \frac{ia_{30}}{z}\frac{L_G}{1+iq}\exp\left[-\beta_0^2 d_3^2/4(1+iq)\right], \tag{16}$$

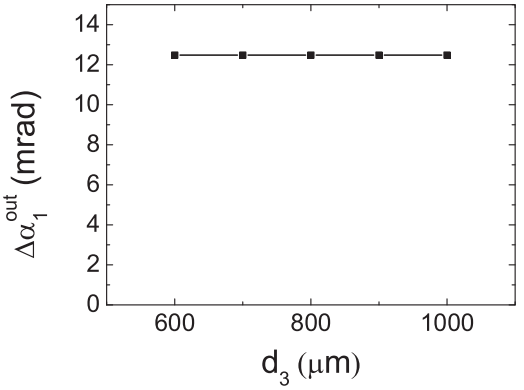

FIG. 7. Dependence of the signal angular spectrum width on pump beam radius. $\alpha_3 = 0.02$ rad, $L_n = 350$ μm, $z = 1$ cm, $\Delta\alpha_1^{in} = 4$ mrad. Solutions of Eqs. (6).

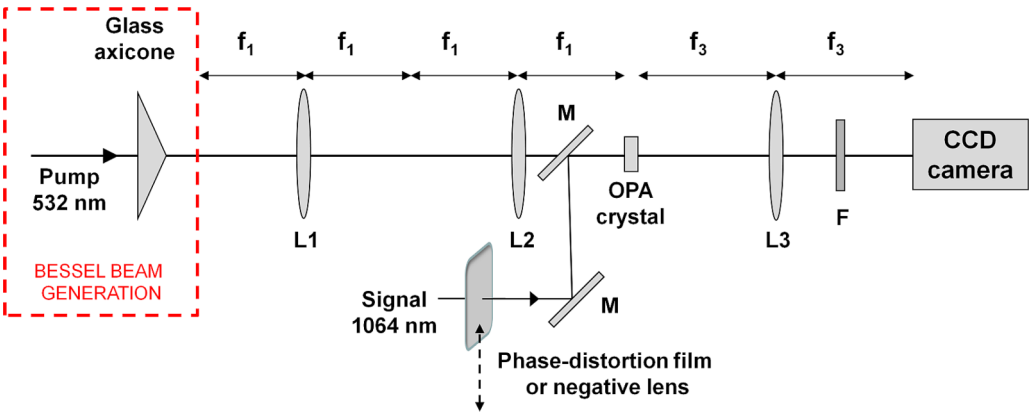

FIG. 8. (Color online) Experimental setup. L1, L2, L3: lenses; M: dichroic mirrors; F: filter.

where $q = L_G/z$ and $L_G = k_3 d_3^2/2$ is a Rayleigh length calculated for the Gaussian envelope of the BG beam. We determine a diffraction length L_B of the BG beam as a distance where an axial intensity of the beam decreases by factor of 2. Thus, we obtain $|A(0,z_B)|^2/a_{30}^2 = 0.5$ and find

$$\frac{q^2}{1+q^2}\exp\left[-\beta_0^2 d_3^2/2(1+q^2)\right] = 0.5. \tag{17}$$

We note that for a good quality BG beam it follows $\beta_0 d_3 \gg 1$. In this case, a solution of Eq. (17) exists only for $q \gg 1$ and, as a result, we obtain

$$L_B \approx \frac{\sqrt{2\ln 2}}{\beta_0 d_3} L_G \approx \frac{0.6 d_3}{\alpha_3}. \tag{18}$$

The diffraction of the BG beam can be neglected at $z \ll L_B$. For $d_3 = 800\ \mu$m and $\alpha_3 = 0.02$ rad, we obtain $L_B = 24$ mm. As we can see from Figs. 3(a) and 4(a), the localization of the signal beam takes place at smaller crystal lengths than L_B.

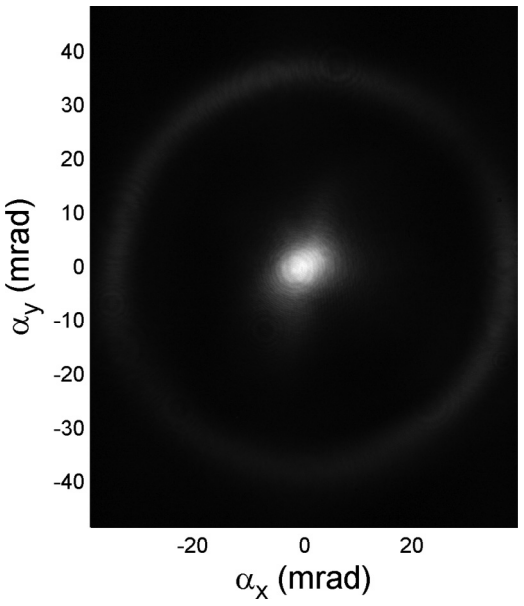

FIG. 9. Intensity distribution of amplification in the OPA radiation in the far field (signal: central spot; idler: ring around it).

III. EXPERIMENTAL DETAILS

The experiment was performed with a diode-pumped Nd:YAG regenerative amplifier (APL 2210B, UAB "Ekspla") producing 50-ps-duration pulses at 1 kHz repetition rate. The Bessel beam was formed using a high-quality glass axicone with the cone angle $2\alpha_3$ equal to 0.04 rad. An experimental setup is presented in Fig. 8. The OPA was pumped by the second harmonic of the Nd:YAG laser ($\lambda = 532$ nm) and seeded by the fundamental harmonic of the same laser. The beam radius before the axicone was 800 μm and the parameter defining the quality of the Bessel beam (ratio of ring radius to ring width) was ~170. The Bessel beam formed by the axicone was imaged to the OPA crystal by two lenses, L1 and L2, of equal focal lengths ($f_1 = 10$ cm). Bessel-beam pulse energy up to 200 μJ was adequate to amplify the seed in the KTP crystal (length 8 mm). The signal was injected into the OPA and type-II interaction close to the noncritical phase matching (KTP crystal orientation $\theta = 0$, $\varphi = 23.2^\circ$) was realized. The far field of the crystal output was imaged by the lens L3 ($f_3 = 15$ cm) onto the CCD camera and angular spectra of parametric waves were registered. The far-field intensity distribution of amplified radiation is shown in Fig. 9, where the central spot denotes an amplified signal and the ring denotes the generated idler wave. The signal beams with different spectrum widths (5–50 mrad) were injected into the

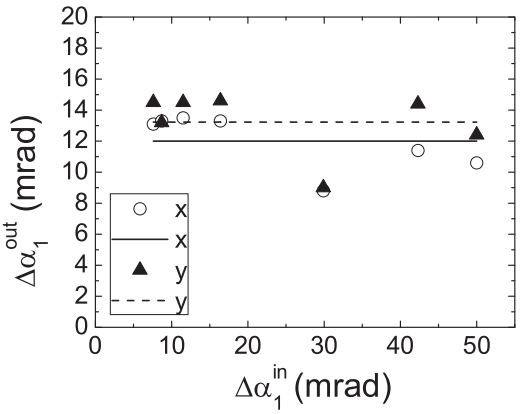

FIG. 10. Angular spectrum width of amplified signal in x and y projections vs angular spectrum width of seed. Circles and triangles: measured data; lines: mean values.

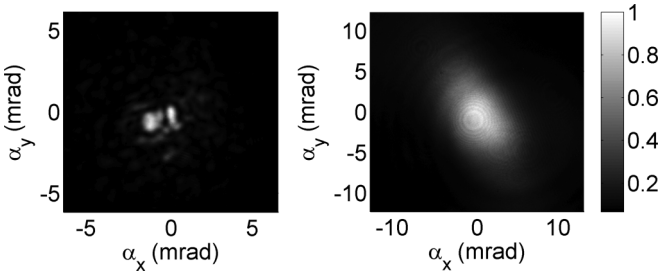

FIG. 11. Amplification of incoherent signal. Normalized angular spectra of signal beam at the input (left) and output (right). Although the input seed was distorted, the amplified signal spectrum is smooth.

OPA and the dependence of the output angular spectrum widths measured at FWHM versus input angular spectrum widths for Bessel pump beam cone angle 0.04 rad is presented in Fig. 10. As can be seen, the angular spectrum width of the amplified radiation does not depend on the spectrum width of the injected signal and remains nearly constant, in agreement with theoretical findings. The obtained angular spectrum width is comparable with the theoretical one; see curve (1) in Fig. 6. The amplification was of the order of one hundred. Finally, we amplified an incoherent signal. The seed was passed through a phase-distortion film before injecting it into the OPA. The film was chosen such that the intensity distribution and angular spectrum of the seed were significantly distorted. The angular spectrum of the injected and amplified signal is depicted in Fig. 11, left and right sides, respectively. As can be seen, while the angular spectrum of the seed is distorted, the distribution of the amplified signal angular spectrum is rather smooth, which is in agreement with the theory. The experimental and theoretical [see Fig. 2(c)] output spectrum widths are comparable, at about 10 mrad.

IV. CONCLUSIONS

It is demonstrated that a signal angular spectrum in the OPA pumped by a Bessel beam after a transient process does not depend on the input signal spectrum and nonlinear crystal length when the pump beam diffraction can be neglected. The signal beam becomes localized in the pump field and is amplified exponentially. As a result, an acceptance angle of the OPA is predefined by the cone angle and intensity of the pump Bessel beam. That takes place also in the case of incoherent input signal beam. A good qualitative agreement between the theoretical and experimental results was obtained.

Note that the parametric amplification in the field of the Bessel pump differs from the amplification in the field of the Gaussian beam. In the case of the Gaussian beam, the acceptance angle of the OPA depends on the crystal length and no localization takes place. The localization property of the OPA pumped by the Bessel beam is determined by transverse phase-matching integral $F(\beta_1,\beta_2)$; see Eq. (7). In this case, the signal beam angular profile depends on the idler angular profile integrated with a kernel $F(\beta_1,\beta_2)$; see Eq. (10). This means that one arrives at the eigenvalue problem and, as a consequence, the localization is obtained. The eigenvalue problem would be destroyed in the case of pump diffraction and depletion, so the localization of the signal beam takes place only when the pump is not depleted and its diffraction can be neglected.

ACKNOWLEDGMENT

This work was partially supported by Research Council of Lithuania, Project No. MIP-073/2013.

[1] J. Durnin, J. Opt. Soc. Am. A **4**, 651 (1987).
[2] D. Mc Gloin and K. Dholakia, Contemp. Phys. **46**, 15 (2005).
[3] T. Wulle and S. Herminghaus, Phys. Rev. Lett. **70**, 1401 (1993).
[4] A. Piskarskas, V. Smilgevičius, A. Stabinis, and V. Vaičaitis, J. Opt. Soc. Am. B **16**, 1566 (1999).
[5] A. Piskarskas, V. Smilgevičius, and A. Stabinis, Opt. Commun. **143**, 72 (1997).
[6] N. V. Belyi, N. S. Kazak, and N. A. Khilo, Opt. Commun. **162**, 169 (1999).
[7] R. Gadonas, A. Marcinkevičius, A. Piskarskas, V. Smilgevičius, and A. Stabinis, Opt. Commun. **146**, 253 (1998).
[8] A. Dubietis, R. Danielius, G. Tamošauskas, and A. Piskarskas, J. Opt. Soc. Am. B **15**, 1135 (1998).
[9] P. Stanislovaitis, A. Narmontas, V. Pyragaite, and V. Smilgevičius, Phys. Rev. A **89**, 043821 (2014).
[10] Y. R. Shen, *The Principles of Nonlinear Optics* (Wiley, Hoboken, NJ, 2003).
[11] A. V. Smith, computer code SNLO (AS-Photonics, Albuquerque, NM, 2012).
[12] R. Loudon, *The Quantum Theory of Light* (Oxford University Press, New York, 2000).
[13] G. Gbur, Opt. Express **14**, 7567 (2006).
[14] M. M. Sushchik, V. M. Fortus, and G. I. Freidman, Radiophys. Quantum Electron. **12**, 235 (1969).
[15] A. P. Sukhorukov and A. K. Shchednova, Sov. Phys. JETP **33**, 677 (1971).
[16] R. Butkus, S. Orlov, A. Piskarskas, V. Smilgevičius, and A. Stabinis, Opt. Commun. **227**, 237 (2003).
[17] S. Orlov, A. Piskarskas, and A. Stabinis, Opt. Lett. **27**, 2103 (2002).
[18] S. Longhi, Phys. Rev. E **69**, 016606 (2004).
[19] M. A. Porras and P. Di Trapani, Phys. Rev. E **69**, 066606 (2004).
[20] S. Orlov, A. Stabinis, V. Smilgevičius, G. Valiulis, and A. Piskarskas, Opt. Lett. **32**, 68 (2007).
[21] F. Gori, G. Guattari, and C. Padovani, Opt. Commun. **64**, 491 (1987).